Transport scaling in an interchange-driven simple magnetized torus

Paolo Ricci*

Centre de Recherches en Physique des Plasmas - École Polytechnique Fédérale de Lausanne, Association EURATOM-Confédération Suisse, CH-1015 Lausanne, Switzerland

B. N. Rogers†

Department of Physics and Astronomy, Dartmouth College, Hanover NH 03755

Abstract

Two-dimensional fluid simulations of a simple magnetized torus are presented, in which the vertical and toroidal components of the magnetic field create helicoidal field lines that terminate on the upper and lower walls of the plasma chamber. The simulations self-consistently evolve the full radial profiles of the electric potential, density, and electron temperature in the presence of three competing effects: the cross-field turbulent transport driven by the interchange instability, parallel losses to the upper and lower walls, and the input of particles and heat by external plasma sources. Considering parameter regimes in which equilibrium $\mathbf{E} \times \mathbf{B}$ shear flow effects are weak, we study the dependence of the plasma profiles – in particular the pressure profile scale length – on the parameters of the system. Analytical scalings are obtained that show remarkable agreement with the simulations.

*Electronic address: paolo.ricci@epfl.ch

†Electronic address: barrett.rogers@dartmouth.edu

I. INTRODUCTION

A simple magnetized torus (SMT) is a plasma confinement device in which vertical and toroidal components of the magnetic field, B_v and B_ϕ, create helicoidal field lines that terminate on the upper and lower walls of the torus vessel. A number of SMTs have now been built (see Refs. [1–3] for some examples) with the goal of exploring the basic physics of turbulent transport in a simple open-fieldline magnetic configuration. Some of these experiments deliver detailed local characterization of the plasma fluctuations and thus offer an excellent test-bed in which to carry out comparisons to numerical simulations [4].

The goal of this work is to explore the self-consistent scaling of the plasma profiles, in particular the pressure gradient scale length, L_p, on the parameters of the device, such as the vertical height and major radius of the chamber, L_v and R, the strength of the plasma sources, and the relative magnitude of B_v and B_ϕ. Linear theory studies and experimental results typically indicate the presence of two main instabilities in the SMT [5]: the interchange mode with $k_{||} = 0$ and driftwaves with $k_{||} \neq 0$. We focus here on parameter regimes in which the turbulent transport in the system is driven predominantly by the interchange mode. Furthermore, we consider parameters typical of the TORPEX experiment [1], i.e. $T_i \ll T_e$ and $\beta \ll 1$, in which the plasma is produced in a radially localized region by microwave injection. The $k_{\|} = 0$ nature of the fluctuations in this case, combined with the relatively high collisionality and low ion temperature typical of the experiments, allows the system to be conveniently studied using two-dimensional, reduced two-fluid simulations that describe field-line averages of the various fluid quantities. Comparisons to three dimensional simulations that include the finite $k_{\|}$ driftwave dynamics, the details of which will be presented in a separate publication, appear to confirm the validity of the two-dimensional model in the regimes studied here. The simulations produce self-consistent, radially-global profiles of the $\mathbf{E}\times\mathbf{B}$ shear, density, and temperature that reflect a balance between external plasma sources, parallel losses to the vacuum chamber, and cross-field turbulent transport due to the interchange modes.

The present work generalizes some of the findings of Ref. [6], which were limited by two key assumptions regarding the parameters of interest: First, it was assumed that the pressure gradient was steep enough to be well away from marginal interchange-mode stability. The second assumption concerns the impact of sheath effects on the longest-wavelength modes

in the system. As the helical fieldlines of the SMT make one full toroidal circuit, they are displaced vertically, in the poloidal plane, by a distance $\Delta = 2\pi R B_v/B_\phi = L_v/N$ where N is the total number of field line turns in the SMT. The $k_\parallel = 0$ assumption imposes vertical periodicity of the system on this scale, and thus sets a maximum vertical perpendicular wavelength $\lambda = \Delta$ or equivalently a minimum vertical wavenumber $k_\Delta = 2\pi/\Delta$. In Ref. [6] it was assumed that sheath effects, which act to cut-off the linear interchange spectrum [6, 7] at wavenumbers below $k \sim k_\sigma$ [where k_σ is defined later in Eq. (4)], were weak even for the smallest $k \sim k_\Delta$ modes allowed in the system: that is, it was assumed that $k_\sigma < k_\Delta$. Here both of these assumptions are relaxed and more general scaling laws are obtained for parameters in which the background $\mathbf{E} \times \mathbf{B}$ shear flow in the system is weak (denoted as the L-mode regime in Ref. [6]).

The present paper is structured as follows: Sec. II presents the model used to describe the interchange turbulence in the SMT. In Sec. III an analytical estimate for L_p is developed, which is compared with the simulation results in Sec. IV. The simulations explore two separate turbulence regimes. In the first, the longest vertical wavelength of the interchange modes is set by sheath boundary condition effects, i.e. $k_\sigma \gg k_\Delta$, while in the second limit the dominant wavelengths in the simulations are fixed by the return of the field line on the poloidal plane, i.e. $k_\sigma < k_\Delta$. Following the Conclusion Section, we present in App. A a derivation of the model used in the paper, while in App. B we briefly summarize the findings obtained in Ref. [6].

II. MODEL

We consider a turbulent regime in which the interchange instability dominates over drift waves, i.e. $D_D/D_I < 1$, where D_D and D_I are the diffusion coefficients due to drift waves and interchange turbulence, respectively. The coefficient D_D can be estimated using a mixing length estimate, $D_D \sim c_s \rho_s^2/L_p$. The estimate of D_I is provided by Eq. (16), and thus one concludes that interchange dynamics overcomes drift wave dynamics if $k_\Gamma \rho_s^2 \left[R/(2L_p^3)\right]^{1/2} / \left[1 - 10L_p/(3R)\right]^{3/2} < 1$, where k_Γ is the vertical wavelength of the mode that contributes most to the transport.

In the regime of interest, owing to the low TORPEX plasma temperature and $k_{||} \simeq$

0, neglecting collisions with neutrals, relatively simple two dimensional equations can be obtained from the drift-reduced Braginskii equations (see, e.g. [8]) to model the plasma dynamics. The details of the derivation are presented in App. A. Here x denotes the radial coordinate, z the coordinate along the magnetic field line, and y the coordinate perpendicular to both x and z. The evolution equations for the line integrated density, $n(x,y,t) = \int n(x,y,z,t)dz/L_c$, potential, $\phi(x,y,t) = \int \phi(x,y,z,t)dz/L_c$, and temperature, $T_e(x,y,t) = \int T_e(x,y,z,t)dz/L_c$, with $L_c = 2\pi NR$ being the magnetic field line length, are:

$$\frac{\partial n}{\partial t} = R\left[\phi, n\right] + 2\left(n\frac{\partial T_e}{\partial y} + T_e\frac{\partial n}{\partial y} - n\frac{\partial \phi}{\partial y}\right) + D\nabla^2 n - \sigma n\sqrt{T_e}\exp\left(\Lambda - \phi/T_e\right) + S_n, \tag{1}$$

$$\frac{\partial \nabla^2\phi}{\partial t} = R\left[\phi, \nabla^2\phi\right] + 2\left(\frac{T_e}{n}\frac{\partial n}{\partial y} + \frac{\partial T_e}{\partial y}\right) + \nu\nabla^4\phi + \sigma\sqrt{T_e}\left[1 - \exp\left(\Lambda - \phi/T_e\right)\right], \tag{2}$$

$$\frac{\partial T_e}{\partial t} = R\left[\phi, T_e\right] + \frac{4}{3}\left(\frac{7}{2}T_e\frac{\partial T_e}{\partial y} + \frac{T_e^2}{n}\frac{\partial n}{\partial y} - T_e\frac{\partial \phi}{\partial y}\right) + k_e\nabla^2 T_e - \frac{2}{3}\sigma\sqrt{T_e^3}\left[1.71\exp\left(\Lambda - \phi/T_e\right) - 0.71\right] + S_T, \tag{3}$$

where $[a,b] = \partial_x a\partial_y b - \partial_y a\partial_x b$, $\Lambda = \log\sqrt{m_i/(2\pi m_e)}$, $\sigma = R/L_c = \Delta/(2\pi L_v)$, and S_n and S_T are the sources in the particle and temperature equations. In Eqs. (1-3) and in the rest of the paper, we normalize n and T_e to reference values n_0 and T_{e0}, time t to R/c_{s0} ($c_{s0} = \sqrt{T_{e0}/m_i}$), lengths to $\rho_{s0} = c_{s0}/\Omega_i$. We note that a system of equations similar to Eqs. (1-3) is used in Ref. [7].

The system of Eqs. (1-3) has been solved numerically, using a numerical code developed from the ESEL code [9], the algorithm of which is described in Ref. [10]. We consider a domain with extension Δ in the vertical direction, and we apply periodic boundary conditions along this direction, due to the flute property of the interchange modes. In the radial direction, we use Dirichlet boundary conditions for the three fields. The source profiles are chosen to mimic the electron cyclotron (EC) and upper hybrid (UH) resonance layer in the TORPEX experiment, i.e., $S_n = S_T = S_0\{S_{UH}\exp\left[-(x - x_{UH})^2/\lambda_{UH}^2\right] + S_{EC}\exp\left[-(x - x_{EC})^2/\lambda_{EC}^2\right]\}$ [11], with $S_{UH} = 1.5$, $S_{EC} = 1$, $\lambda_{UH} = 5$, $\lambda_{EC} = 2.5$, $x_{UH} = 35$, $x_{EC} = 15$.

The simulations are started from random noise. The sources then introduce plasma and heat, increasing the plasma pressure and triggering the interchange instability. The interchange instability leads to density and particle transport in the radial direction from the source region to the low field side of the machine; at the same time, plasma is removed from the system by parallel losses. The results discussed in the present paper focus on the quasi-steady state period, established after an initial transient phase, resulting from a balance between parallel losses, perpendicular transport, and the sources.

As summarized in App. B, the plasma dynamics described by the model (1-3) has been discussed in Ref. [6] in configurations far from marginal stability and $k_\sigma < k_\Delta$. The presence of two turbulence regimes was pointed out. The high confinement regime (H mode) is characterized by a strong shear flow, i.e. $\gamma/v'_{\mathbf{E}\times\mathbf{B}} < 0.5$, where γ is the peak linear growth rate of the interchange mode, and $v'_{\mathbf{E}\times\mathbf{B}} = R\partial_x^2\phi$ is the $\mathbf{E}\times\mathbf{B}$ shear flow. Shear flow creates a transport barrier that limits the perpendicular transport, steepening up the plasma profiles and increasing the peak plasma pressure. We focus here instead on the low confinement regime (L mode), where shear flow plays a negligible role and plasma transport occurs freely in the radial direction; thus, for the simulations presented $\gamma/v'_{\mathbf{E}\times\mathbf{B}} > 0.5$.

III. THEORETICAL ESTIMATE OF L_p

We first note that the maximum of the local linear growth rates associated to Eqs. (1-3) occurs for $k_y \simeq k_\sigma$ where

$$k_\sigma = \sqrt{\frac{\sigma}{\gamma\sqrt{T_e}}}. \tag{4}$$

Sheath effects suppress the linear growth rates at long wavelengths $k_y < k_\sigma$, while ρ_s effects decrease the growth rates at shorter wavelengths.

First we restrict attention to parameters for which sheath effects do not strongly influence the dynamics of the $k_y = k_\Gamma$ interchange mode, where k_Γ denotes the wavenumber of the mode that provides the dominant contribution to the transport. The analysis of the linearized system of Eqs. (1-3) shows that this occurs for $\sigma < \gamma/\sqrt{T_e}$ and $k_\Gamma\sqrt{T_e} > \max\{\sigma, k_\sigma\sqrt{T_e}\}$. Moreover, we consider cases in which ρ_s effects do not strongly influence the linear properties of the k_Γ mode: this occurs when $k_\Gamma\sqrt{T_e} < \gamma/\sqrt{T_e}$.

As we now show, the balance between plasma parallel losses and perpendicular transport

leads to an expression for the pressure scale length, $L_p = |\overline{p}/\partial_x \overline{p}|$ (the analogous definition is used for L_n and L_T). The overbar denotes the time average of the physical quantities, the tilde the fluctuating part (e.g., $p = \overline{p} + \tilde{p}$). By multiplying Eqs. (1) and (3) by T_e and n, respectively, considering the time and y average of their sum, and noting that $\tilde{p}/\overline{p} \simeq \tilde{T}_e/\overline{T}_e + \tilde{n}/\overline{n}$, the balance between parallel and perpendicular transport yields

$$\frac{\partial \Gamma_p}{\partial x} = -\frac{5}{3}\sigma \overline{p}\,\overline{T}_e^{1/2} \tag{5}$$

in the source free region where the time and y averaged cross-field radial transport is given by $\Gamma_p = R\left\langle \overline{\tilde{p}\partial_y \tilde{\phi}} \right\rangle_y$.

We first estimate $\partial_y \tilde{\phi}$. In the regime of interest it is possible to neglect sheath terms and the dominant terms in Eq. (1) lead to

$$\frac{\partial \tilde{n}}{\partial t} \simeq R\left[\phi, n\right] - 2n\frac{\partial \tilde{\phi}}{\partial y} \simeq \overline{n}\frac{\partial \tilde{\phi}}{\partial y}\left(\frac{R}{L_n} - 2\right) \tag{6}$$

and a similar expression can be deduced from Eq. (3) for the temperature

$$\frac{\partial \tilde{T}_e}{\partial t} \simeq R\left[\phi, T_e\right] - \frac{4T_e}{3}\frac{\partial \tilde{\phi}}{\partial y} \simeq \overline{T}_e\frac{\partial \tilde{\phi}}{\partial y}\left(\frac{R}{L_T} - \frac{4}{3}\right). \tag{7}$$

By summing Eqs. (6) and (7), and approximating $\partial_t \tilde{n} \sim \gamma \tilde{n}$ and $\partial_t \tilde{T}_e \sim \gamma \tilde{T}_e$, one obtains

$$\frac{\partial \tilde{\phi}}{\partial y} \sim \gamma \frac{\tilde{p}}{R\partial_x \overline{p} - 10\overline{p}/3} \tag{8}$$

which is the desired expression for $\partial_y \tilde{\phi}$. As a consequence of Eqs. (7) and (8) one also obtains $L_T = 5L_p/2$ and $L_n = 5L_p/3$.

We now turn to the estimate of $\tilde{p}$. The turbulence saturates when the unstable modes become strong enough to neutralize the main source of free-energy in the system; i.e., when $\partial_x \tilde{p}$ is able to relax the equilibrium gradient to its marginally stable value. We evaluate $\partial_x \tilde{p}$ using standard non-local linear theory methods (employed for example in Ref. [12] for drift waves) that are valid for $k_\Gamma L_p > 1$. By linearizing the system (1-3), one can express $\tilde{n}$ and $\tilde{T}_e$ as a function of $\tilde{\phi}$. An eigenvalue equation for $\tilde{\phi}$ is then found, $\partial_x^2 \tilde{\phi} - k_y^2\left[1 + G(x)\right]\tilde{\phi} = 0$, where

$$G(x) = \frac{2}{n}\frac{3R\gamma\partial_x p + 10\gamma p - 10ik_y T_e^2(R\partial_x n + 2n)}{\gamma\left(3\gamma^2 - 20ik_y T_e\gamma - 20k_y^2 T_e^2\right)} \simeq \frac{2}{n\gamma^2}\left(R\frac{\partial p}{\partial x} + \frac{10}{3}p\right) \tag{9}$$

within the small $k_y\sqrt{T_e}$ approximation. Taylor-expanding $G(x) \simeq G_0 + G_0''(x-x_0)^2/2$, with x_0 the point of instantaneous steepest pressure gradient, $G_0 = G(x_0)$, and

$$G_0'' = \left.\frac{\partial^2 G(x)}{\partial x^2}\right|_{x=x_0} \sim \frac{2RT_e(10/3 - R/L_p)}{\gamma^2 L_p^3} \tag{10}$$

one is lead to a harmonic oscillator equation for $\tilde{\phi}$. In the limit $k_y L_p > 1$, one has $\gamma \simeq \gamma|_{x=x_0}$, given by the solution of the equation $1 + G(x_0) = 0$, and $\tilde{\phi} \propto \exp[-a(x-x_0)^2/2]$ with $a = k_y\sqrt{|G_0''|/2}$. We note that the equation $1 + G(x_0) = 0$ provides the local dispersion relation of our model in the regime of interest, and can be written as

$$\gamma^3 - \frac{20}{3} i k_y T_e \gamma^2 - \left[\frac{20T_e}{3}\left(T_e k_y^2 - 1\right) + \frac{2T_e R}{L_p}\right]\gamma - \frac{20}{3} i k_y T_e^2 \left(2 - \frac{R}{L_n}\right) = 0 \tag{11}$$

which coincides with the dispersion relation in Ref. [13] in the limit $T_i \to 0$. Two instabilities are contained in the dispersion relation (11). In the limit $\gamma \sim \sqrt{T_e}$ and $k_\Gamma\sqrt{T_e} < 1$ one obtains the dispersion relation of the interchange mode

$$\gamma = \sqrt{T_e\left(\frac{2R}{L_p} - \frac{20}{3}\right)} \tag{12}$$

with a critical pressure gradient $L_p/R = 3/10$. If one instead scales $\gamma \sim T_e k_y$, the dispersion relation for the entropy mode is obtained. For $k_y\sqrt{T_e} < 1$ it can be written as $\gamma = 10 i k_y T_e(2 - R/L_n)/(3R/L_p - 10)$ and thus the entropy mode is stable in the present configuration [13]. Focusing on the interchange mode, the typical radial extension of the instability is thus given by $1/\sqrt{a} \sim \sqrt{L_p/k_y}$ and considering the dominant mode, $k_y = k_\Gamma$, one estimates $\partial_x\tilde{n} \sim \sqrt{k_\Gamma/L_p}\tilde{n}$ and $\partial_x\tilde{T}_e \sim \sqrt{k_\Gamma/L_p}\tilde{T}_e$ from which $\partial_x\tilde{p} \sim \sqrt{k_\Gamma/L_p}\tilde{p}$

As noted earlier saturation occurs when the turbulent fluctuations effectively remove the instability drive from the system. We can model this as

$$\partial_x\tilde{p} \sim \partial_x\bar{p}\left(1 - \frac{10}{3}\frac{L_p}{R}\right) \ . \tag{13}$$

The factor on the right-hand side vanishes as marginal interchange stability is approached - an effect that was not included in Ref. [6] due to the assumption $L_p \gg R$. We will show in Sec. IV that the analytic estimates following from Eq. (13) yield good agreement with the simulations even near marginal stability. We obtain

$$\tilde{p} \sim \sqrt{\frac{L_p}{k_\Gamma}}\frac{\bar{p}}{L_p}\left(1 - \frac{10}{3}\frac{L_p}{R}\right) \tag{14}$$

Using the results from Eqs. (8) and (14), one can thus evaluate

$$\Gamma_p = \alpha \sqrt{\frac{2\overline{T}_e R}{L_p}} \frac{\overline{p}}{k_\Gamma} \left(1 - \frac{10}{3}\frac{L_p}{R}\right)^{3/2} \tag{15}$$

where α is a numerical parameter determined from simulation data ($\alpha \simeq 0.34$). Defining a diffusion coefficient for the interchange mode as $D_I = \Gamma_p / \partial_x \overline{p}$, one has that

$$D_I = \alpha \frac{\sqrt{2\overline{T}_e R L_p}}{k_\Gamma} \left(1 - \frac{10}{3}\frac{L_p}{R}\right)^{3/2} \tag{16}$$

Inserting the expression for Γ_p given in Eq. (15) into Eq. (5), since $\partial_x(\overline{T}_e^{1/2}\overline{p}) = -6\overline{T}_e^{1/2}\overline{p}/5$, one finally obtains the desired equation for L_p

$$\alpha \sqrt{\frac{2R}{L_p^3}} \left(1 - \frac{10}{3}\frac{L_p}{R}\right)^{3/2} = \frac{25}{18}\sigma k_\Gamma \tag{17}$$

IV. COMPARISON WITH SIMULATION RESULTS

We consider two regimes in which to compare Eq. (17) to the simulation results. We first examine the case $k_\Delta \ll k_\sigma$. In this regime, the dominant modes (e.g. the modes with the largest growth rates) have wavenumbers dictated by the sheath dynamics: $k_\Gamma \sim k_\sigma$, and have corresponding wavelengths that are smaller than Δ. In the second regime of interest, we assume $k_\Delta > k_\sigma$ and thus the strongest, fastest growing modes in the system are governed by the box size: $k_\Gamma = k_\Delta$.

The parameter space of the two regimes can be estimated as follows. Introducing $\kappa = k_\Delta / k_\sigma$, the T_e value in Eq. (4) can be evaluated as the maximum temperature $T_{e,max}$ in the system. The global temperature balance from Eq. (3) then leads to [6]

$$T_{e,max}^{3/2} \simeq \frac{\int S_T dx}{\sigma(2\xi x_S/3 + 4L_T/9)} \tag{18}$$

where $\xi \simeq 0.5$ and x_S denotes the location of the peak temperature, corresponding to the source position ($x_S \simeq 36$ in the present simulations). Thus, one can write

$$\kappa = \frac{2\pi}{\Delta} \left(\frac{\int S_T dx}{2\xi x_S/3 + 4L_T/9}\right)^{1/3} \frac{1}{\sigma^{5/6}} \sqrt{\frac{2R}{L_p} - \frac{20}{3}} \tag{19}$$

being the regime $k_\Delta \ll k_\sigma$ attained for $\kappa \ll 1$, while $k_\Delta > k_\sigma$ implies $\kappa > 1$.

A. $k_\Delta \ll k_\sigma$

We perform a number of simulations in the $k_\Delta \ll k_\sigma$ regime, varying the source strength, S_0, σ, and R and we evaluate L_p by measuring the distance between p_{max} and $p_{max}/2$. All the simulations performed show that the mode predominantly contributing to the transport has a wavelength comparable to that of the peak growth rate, k_σ; precisely, it is found that $k_\Gamma = \zeta k_\sigma$, with $\zeta \simeq 1.5$. The half width half maximum of the spectrum is typically $0.4 k_\sigma$. From Eq. (17), the following equation for L_p is obtained

$$\frac{\alpha}{2}\left(\frac{2R}{L_p}\right)^{7/4}\left(1-\frac{10}{3}\frac{L_p}{R}\right)^{7/4} = \zeta R \sigma^{11/6}\frac{25}{18}\left[\frac{2\xi x_S/3 + 10 L_p/9}{\int S_T dx}\right]^{1/3} \tag{20}$$

Note that $0 < L_p < 3R/10$ and marginal stability is reached for $\sigma \to 0$ or $\int S_T dx \to \infty$.

The dependence of L_p on σ and S_0 (for $R = 200$) is shown in Fig. 1, where the prediction of Eq. (20) are compared with the simulation results, showing remarkable agreement. The L_p dependence on R is shown in Fig. 2 (with $S_0 = 1$ and $\sigma = 0.1$ fixed).

We note that, since k_σ depends on the local value of T_e, L_p is not constant. In particular, the estimate given by Eq. (20) for L_p is valid close to the pressure peak, where $\overline{T}_e \simeq T_{e,max}$.

B. $k_\Delta > k_\sigma$

Imposing $k_\Gamma = k_\Delta$, Eq. (17) becomes

$$\alpha\sqrt{\frac{2R^3}{L_p^3}}\left(1-\frac{10}{3}\frac{L_p}{R}\right)^{3/2} = \frac{25}{18}\frac{R}{L_v} \tag{21}$$

showing that L_p/R depends only on the geometrical parameters of the SMT, i.e. L_v/R. We note that two limits are present in this dispersion relation. In the case $L_v \ll R$, Eq. (21) provides $L_p \propto (L_v\sqrt{R})^{2/3}$, which matches the L_p estimate in Ref. [6], as summarized in App. B. Instead, if $L_v \gg R$, one obtains $L_p = 3R/10$, the marginal stability threshold for the interchange mode. The simulation results in the $k_\Delta > k_\sigma$ regime are shown in Fig. 3. Simulations and analytical theory again show good agreement.

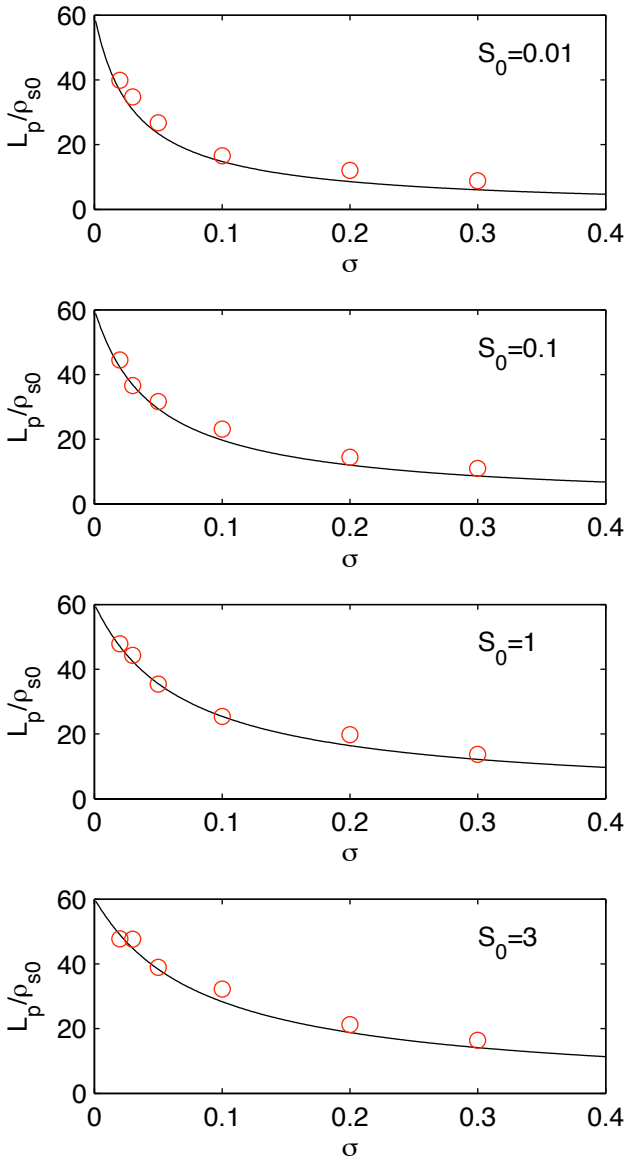

FIG. 1: (Color online) L_p as a function of σ and different value of S_0 from Eq. (20) (black line) and simulation value (red circles). $R = 200$.

V. CONCLUSIONS

In the present paper, the dependence of L_p on the geometrical parameters of the SMT, the plasma source strength, and the magnetic configuration has been obtained. The estimate provides a theory-based prediction that may be compared and checked against SMT experiments with different dimensions.

In the case of the TORPEX device [1], experiments have been performed by varying the

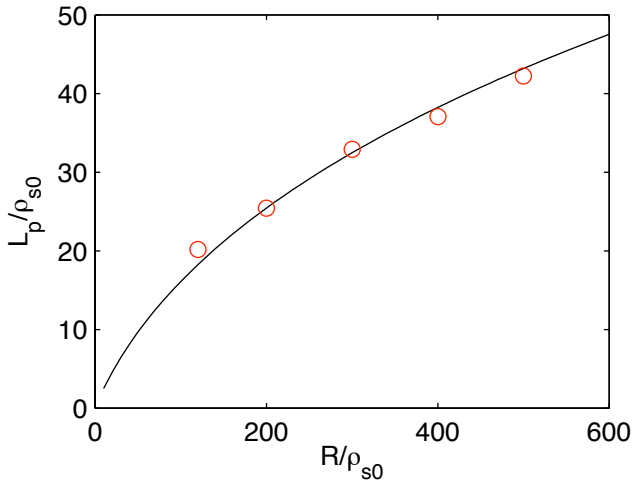

FIG. 2: (Color online) L_p as a function of R as predicted by Eq. (20) (black line) and simulation results (red circles). $S_n = 1$ and $\sigma = 0.1$.

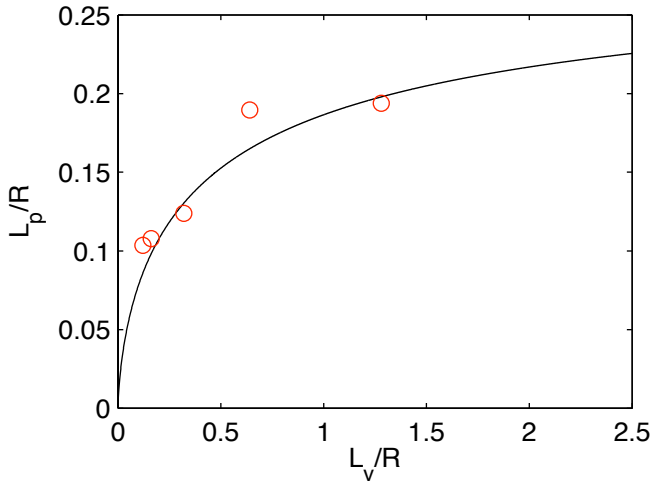

FIG. 3: (Color online) L_p/R as a function of L_v/R as predicted by Eq. (21) (black line) and simulation results (red circles).

value of B_z in the $k_\Delta > k_\sigma$ regime [5]. It has been shown that L_n and L_T are not strongly affected by the B_z field, as expected from Eq. (21). The L_T/L_n ratio is close to the 3/2 predicted theoretically and a L_p/R in the range $0.05 - 0.07$ is measured [5, 14]. TORPEX is characterized by a circular poloidal cross section, with the ratio L_v/R varying with the radius and having its maximum at the center of the cross section, $L_v/R = 0.4$. According

to Fig. 3, $L_v/R = 0.4$ corresponds to $L_p/R \simeq 0.14$. Thus, the estimate presented in the present paper seems to be in reasonable agreement with the experimental measurements. The Helimak experiment [2] is characterized by a rectangular cross section, with $L_v/R \simeq 2$. In this device, typical measurements lead to L_p/R in the range $0.15 - 0.2$ [15]. In good agreement with the experimental measurements, for $L_v/R = 2$, Fig. 3 yields $L_p/R \simeq 0.22$.

Acknowledgments

We gratefully acknowledge many useful discussions with A. Fasoli, I. Furno, B. Labit, M. Podestà, and C. Theiler, as well as K. Gentle and B. Li for providing the pressure scale length relative to the Helimak experiment. P.R. was supported by a EURATOM fusion fellowship.

Appendix A: Deduction of the two-dimensional model for interchange turbulence

In the case of constant magnetic curvature equal to R, the drift-reduced Braginskii equations [8] for $n(x, y, z, t)$, $T_e(x, y, z, t)$ and $\phi(x, y, z, t)$ can be written as

$$\frac{\partial n}{\partial t} = R\left[\phi, n\right] + 2\left(n\frac{\partial T_e}{\partial y} + T_e\frac{\partial n}{\partial y} - en\frac{\partial \phi}{\partial y}\right) + D_n\nabla_\perp^2 n - \frac{\partial (nV_{||e})}{\partial z} + S_n \tag{A1}$$

$$\nabla\cdot(n\mathbf{v}_{pol}) = -2\left(\frac{T_e}{n}\frac{\partial n}{\partial y} + \frac{\partial T_e}{\partial y}\right) - \frac{1}{n}\frac{\partial j_{||}}{\partial z} + \frac{\eta_{0i}}{n}\left(2\frac{\partial^2 V_{||i}}{\partial y\partial z} - \frac{\partial^2\phi}{\partial y^2}\right) - D_\phi\nabla_\perp^4\phi \tag{A2}$$

$$\frac{\partial T_e}{\partial t} = R\left[\phi, T_e\right] - V_{||e}\frac{\partial T_e}{\partial z} + \frac{4}{3}\left(\frac{7}{2}T_e\frac{\partial T_e}{\partial y} + \frac{T_e^2}{n}\frac{\partial n}{\partial y} - T_e\frac{\partial\phi}{\partial y}\right) + D_T\nabla_\perp^2 T_e + \frac{2}{3}\frac{T_e}{n}0.71\frac{\partial j_{||}}{\partial z} - \frac{2}{3}T_e\frac{\partial V_{||e}}{\partial z} + S_T \tag{A3}$$

where η_{0i} is the Braginskii viscosity. We simplify Eq. (A2) by using the Boussinesq approximation for the polarization drift [16]

$$\nabla \cdot (n\mathbf{v}_{pol}) = R\left[\phi, \nabla_\perp^2 \phi\right] - \frac{\partial \nabla_\perp^2 \phi}{\partial t} - V_{||i}\frac{\partial \nabla^2 \phi}{\partial z} \tag{A4}$$

Reference [17] shows that the ion parallel flow at the sheath edges, $z = \pm L_c/2$, can be approximated as $nV_{||i}\big|_{z=\pm L_c/2} \simeq \pm n\sqrt{T_e}/2\big|_{z=0}$, and the electron flow as $nV_{||e}\big|_{z=\pm L_c/2} \simeq \pm n\sqrt{T_e}\exp(\Lambda - \phi/T_e)/2$. By integrating Eqs. (A1-A3) along the z direction from $-L_c/2$ to $L_c/2$, using the expressions for the electron and ion flux at the sheath edges, neglecting the η_{0i} terms and the z-dependence of n, ϕ, and T_e, the two-dimensional fluid equations Eqs. (1-3) that describe the plasma turbulence in our system are deduced.

Appendix B: Brief summary of the main findings in the regime far from marginal stability and $k_\Delta > k_\sigma$

We briefly summarize the findings of Ref. [6] that examines configurations far from marginal stability and having $k_\Delta > k_\sigma$, i.e. $k_\Gamma = k_\Delta$. Far from marginal stability, $L_n \ll R$ and the leading order terms in Eq. (1) are $\partial_t n - R[\phi, n] \simeq 0$ from which, in the absence of a strong shear flow, one has $\partial_y \tilde{\phi} \sim \gamma_0 \tilde{n}/(R\partial_x \overline{n})$ with $\gamma_0 = \sqrt{2T_e R/L_p}$. Turbulence saturation occurs for $\partial_x \overline{n} = \partial_x \tilde{n}$. The $\partial_x \tilde{n}$ term can be estimated by the nonlocal linear theory outlined in Sec. III, obtaining $\tilde{n} \sim \overline{n}(L_p/k_\Delta)^{1/2}/L_n$. Thus, $\Gamma_n = R\left\langle \overline{\tilde{n}\partial_y \tilde{\phi}} \right\rangle_y \sim \overline{n}(2RL_p\overline{T}_e)^{1/2}/(L_n k_\Delta)$ and, analogously, $\Gamma_T = R\left\langle \overline{\tilde{T}_e \partial_y \tilde{\phi}} \right\rangle_y \sim (2RL_p\overline{T}_e^3)^{1/2}/(L_n k_\Delta)$. The expression for Γ_n and Γ_T can be inserted into the y and time-averaged Eq. (1) and Eq. (3) that in the source free region read

$$\frac{\partial \Gamma_n}{\partial x} \simeq -\sigma \overline{n}\overline{T}_e^{1/2}, \frac{\partial \Gamma_T}{\partial x} \simeq -\frac{2}{3}\sigma \overline{T}_e^{3/2}, \tag{B1}$$

thus obtaining $L_n \propto (L_v\sqrt{R})^{2/3}$ and $L_T \propto (L_v\sqrt{R})^{2/3}$. In Ref. [6], the presence of a turbulence regime was observed, where shear flow limits the perpendicular transport, steepening the plasma profiles. This regime was denoted as high confinement mode (H mode) regime and it appears when $\gamma_0/v'_{\mathbf{E}\times\mathbf{B}} < 0.5$.

We now estimate the L-H threshold condition. Shear flow amplitude is limited by the Kelvin-Helmholtz instability; in general, the maximum allowed shear flow is present in the simulations, i.e. $v'_{\mathbf{E}\times\mathbf{B}} \simeq \chi\phi_{max}/\Delta^2$, with $\chi \simeq 2.5$. Since it is observed that

$L_T \simeq L_n \simeq \Delta$ at the L-H threshold, the transition condition, $\gamma_0/v'_{\mathbf{E}\times\mathbf{B}} \simeq 0.5$, can be rewritten as $2\Delta^{3/2}/(\chi\Lambda\sqrt{RT_{e,max}}) \simeq 0.5$. The value of $T_{e,max}$ can be estimated from Eq. (18) and one deduces that the L-H transition occurs for

$$\frac{2\Delta^{11/6}}{\chi\Lambda\sqrt{R}}\left(\frac{4/9\Delta + 2\xi x_S/3}{2\pi L_v \int S_T dx}\right)^{1/3} \simeq 0.5. \tag{B2}$$

---

[1] A. Fasoli, B. Labit, M. McGrath, S. H. Müller, G. Plyushchev, M. Podestà, and F. M. Poli, Phys. Plasmas **13**, 055902 (2006).

[2] J.C. Perez, W. Horton, K. Gentle, W. L. Rowan, K. Lee, and R. B. Dahlburg, Phys. Plasmas **13**, 032101 (2006); K.W. Gentle and H. Huang, Plasma Science and Technology **10**, 284 (2008).

[3] E.D. Zimmerman and S.C. Luckhardt, J. Fusion Energy **12**, 289 (1993); K. Rypdal and S. Ratynskaia, Phys. Rev. Lett. **94**, 225002 (2005); P.K. Sharma and D. Bora, Plasma Phys. Control. Fusion **37**, 1003 (1995); C. Riccardi, M. Fontanesi, A. Galassi, and E. Sindoni, Plasma Phys. Control. Fusion, **36**, 1791 (1994).

[4] P. Ricci, C. Theiler, A. Fasoli, I. Furno, B. Labit, S. H. Müller, M. Podesttà, and F. M. Poli, Phys. Plasmas **16**, 055703 (2009).

[5] F.M. Poli, P. Ricci, A Fasoli, M. Podestà, Phys. Plasmas **15**, 032104 (2008).

[6] P. Ricci, B.N Rogers, and S. Brunner, Phys. Rev. Lett. **100**, 225002 (2008).

[7] N. Bisai, A. Das, S. Deshpande, R. Jha, P. Kaw, A. Sen, and R. Singh, Phys. Plasmas **11**, 4018 (2004).

[8] A. Zeiler, J.F. Drake, and B. Rogers, Phys. Plasmas **4**, 2134 (1997).

[9] V. Naulin, J. Nycander; J.J. Rasmussen, Phys. Rev. Lett. **81**, 4148 (1998); O.E. Garcia, V. Naulin, A.H. Nielsen, and J. J. Rasmussen, Phys. Rev. Lett. **92**, 165003 (2004).

[10] V. Naulin and A.H. Nielsen, Siam J. Sci. Comput. **25**, 104 (2003).

[11] M. Podestà, A. Fasoli, B. Labit, M. McGrath, S.H. Müller, and F.M. Poli, Plasma Phys. Control. Fusion **48**, 1053 (2006).

[12] B.N. Rogers and W. Dorland, Phys. Plasmas **12**, 062511 (2005).

[13] P. Ricci, B. N. Rogers, W. Dorland, and M. Barnes, Phys. Plasmas **13**, 062102 (2006).

[14] I. Furno, B. Labit, M. Podestà, A. Fasoli, S. H. Müller, F. M. Poli, P. Ricci, C. Theiler, S. Brunner, A. Diallo, and J. Graves, Phys. Rev. Lett. **100**, 055004 (2008).

[15] K. Gentle and B. Li (private communication, 2009).

[16] C.Q. Yu, S. I. Krasheninnikov, and P. N. Guzdar, Phys. Plasmas **13**, 042508 (2006).

[17] P.C. Stangeby, The plasma boundary of magnetic fusion devices, IOP publishing (2000).